One-Dimensional Transient Model for Frost Heave in Polymer Electrolyte Fuel Cells : I. Physical Model

Suhao He and Matthew M. Mench

J. Electrochem. Soc. 2006, Volume 153, Issue 9, Pages A1724-A1731.
doi: 10.1149/1.2216547

Journal of The Electrochemical Society, **153** (9) A1724-A1731 (2006)
0013-4651/2006/153(9)/A1724/8/$20.00 © The Electrochemical Society

One-Dimensional Transient Model for Frost Heave in Polymer Electrolyte Fuel Cells

I. Physical Model

Suhao He* **and Matthew M. Mench****,z**

Fuel Cell Dynamics and Diagnostics Laboratory, and Department of Mechanical and Nuclear Engineering, The Pennsylvania State University, University Park, Pennsylvania 16802, USA

To better understand, control, and mitigate degradation during freezing of a polymer electrolyte fuel cells (PEFCs), a one-dimensional (1D) transient model has been formulated, based on theories of porous media flow and soil frost heave. The model is essentially a modified hybrid of Harlan's hydraulic model and Miller's rigid ice model with additional improvements for suitable application to PEFCs. It is found that the three types of characteristic curves for unfrozen water flow and frost heave modeling can be well unified. Methods to derive the unfrozen water vs temperature characteristic curves for PEFC components are also given. Through the formulated model, it is predicted that ice lens will occur most likely around the catalyst layer, either between catalyst layer and diffusion media, or between catalyst layer and Nafion membrane. Lens formation under the lands is unlikely due to high overburden pressure. Ice lens growth may explain breakthrough observed in carbon paper after freeze-thaw tests. Another phenomenon, the delamination between Nafion and catalyst layer, can possibly be explained by the formation of an ice lens from water expelled from the electrolyte during freezing. The Nafion thickness and initial water content have direct impact on the damage in this mode.
 [DOI: 10.1149/1.2216547]

Manuscript submitted November 10, 2005; revised manuscript received April 27, 2006. Available electronically July 17, 2006.

The freezing/thawing behavior of polymer electrolyte fuel cells (PEFCs) is relatively a new topic in fuel cell science and technology, with only a few published papers, presentations, and reports to date regarding freeze-thaw induced damage.[1-11] Besides these, Pesaran et al.[12] summarized some of the most recent developments in this field. From this open literature, there exist some conflicting claims whether there is possible damage during the freeze-thaw operation. Some groups found no performance loss after freeze-thaw cycling.[1-3] Among them, Wilson et al.[1] cycled from −10 to 80°C, while McDonald et al.[2] and Blair[3] cycled from −40 to 80°C. Pivovar et al.[4] also cycled down to −40°C and did not find performance loss, but when they cycled from −80°C, they observed delamination of the catalyst layer from the membrane. Some other groups observed some damages.[5-8] Cho et al.[5,6] cycled from −10 to 80°C. They found that, when the degradation is occurring, the cell impedance increased, and the active electrochemical area decreased concomitant with increasing pore size in the catalyst layer. They concluded that the degradation is related to the residual water in the PEFC. After purging the PEFC, or supplying an anti-freezing solution after cell shutdown, they found the short-term degradation could be prevented. Meyers[7] cycled from −20°C and observed membrane failure and catalyst delamination from the membrane. Gaylord[8] also showed pictures illustrating membrane failure and breakthrough of the carbon paper after freeze-thaw tests. We believe the current lack of comprehensive modeling or experimental data to explain the difference is probably the factor differentiating these seemly conflicting results. From these literature, three physical modes of damage can be documented: membrane failure, delamination between membrane and catalyst, and breakthrough of the diffusion media. However, even the fundamental mechanisms that cause these modes of damage during freeze-thaw cycling are still unclear. A goal of this work is to explain the last two modes of physical degradation so that suitable mitigation can be achieved.

In soil science, researchers have studied the frost heave phenomenon continuously during the last century. Frost heave occurs during the winter and early springtime in cold climates. The noticeable heaving induces uneven support of pavement, forming cracks in the pavement surface layer, which look similar to "mudcracking" observed in the diffusion media and catalyst layer in some PEFC tests.[4,7,8] In the past, people believed the frost heave was a result of the expansion of water during freezing. It was later proved experimentally that thermal and mass transport plays a major role during the process, and heave can occur even for a substance that contracts on freezing.[13-15] Frost heave is divided into primary heave and secondary heave, depending on whether there is a frozen fringe. As shown in Fig. 1, the frozen fringe is a two-phase zone where ice content increases from 0% at the freezing front to 100% at the location of the lens.[16] The temperature-induced freezing changes the capillary force distribution in the soil and, in response, moisture redistributes and is transported to the freezing front, forming ice lenses. The growth of lenses below the soil surface can heave soil upward whenever certain criteria are met. Reviews from O'Neill[17] and Black and Haradenberg[18] are good references for further reading. Most recent developments can be found in paper by Nakano.[19]

There are two distinct paths in the historical development of theoretical models for frost heave and unfrozen water flow in soil, treated as porous media. Miller,[20] O'Neill and Miller,[21] and Black[22] developed a well-known frost heave model for saturated soil, the rigid ice model. In their model, they proposed that the ice lens growth is due to the regelation process, or refreezing motion. The rigid ice model is based on the generalized Clapeyron equation (GCE), developed by Loch[23] and reviewed by Henry.[24] The GCE describes the thermodynamic equilibrium between pore ice and unfrozen water distributed in the fringe. However, the validity of this relation has been disputed. Førland et al.[25] believed that irreversible thermodynamics should be applied for frost heave modeling. According to Newman and Wilson,[26] the GCE may not apply to soils

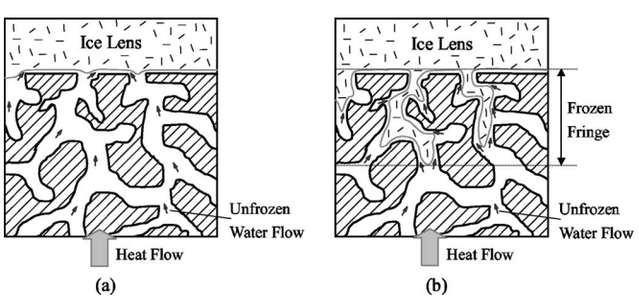

Figure 1. Comparison of (a) primary and (b) secondary frost heave, following Ref. 16.

* Electrochemical Society Student Member.
** Electrochemical Society Active Member.
z E-mail: mmm124@psu.edu

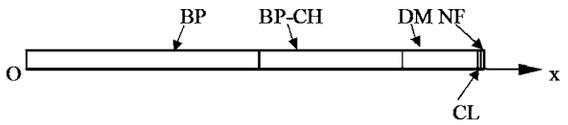

Figure 2. 1D model PEFC geometry.

containing both capillary and adsorptive water forces. However, the GCE was later used by Selvadurai et al.[27] to develop a 3-D frost heave model. Most recently, Rempel et al.[28] modified the GCE by adding the disjoining pressure, through which they determined the fluid pressure from integral force balance.

Harlan[29] took another approach to model unfrozen water flow. He used a hydraulic model, assuming that a single suction force can be used to account all the capillary effects, and that the permeability vs saturation relation is the same for a partially frozen soil and an unfrozen unsaturated soil. But experimental validation shows that the model overpredicted ice accumulated behind the frost front. Jame and Norum[14] modified the model by adding an adjustable impedance factor to the permeability expression to account for effects of ice. The hydraulic model was later extended by several researchers to model unsaturated freezing, because of its numerical simplicity.[26,30-32] Recently, by using a functional relationship for permeability vs capillary pressure proposed by Fredlund et al.,[33] Newman and Wilson[26] claimed that they could calculate the exact water distribution without use of the arbitrary impedance factor for calibrating the permeability function.

The hydraulic model is relatively straightforward to apply, but it cannot predict the ice lens formation well, since it does not include a physical mechanism. For the rigid ice model, ice lens formation occurs when the overburden pressure is overcome, which is more reasonable. The overburden pressure is a term used in geology to denote the pressure on the ice lens induced by soil weight, since an ice lens will bear the full load being lifted by heave.[21] However, this model only provides the phase pressure balance between ice and liquid water, which is not sufficient to describe the influence of the air phase during unsaturated freezing. Thus, the rigid ice model is useful only for frost heave modeling in completely saturated porous media, while both saturated and unsaturated domains would exist in a typical PEFC diffusion media and catalyst layer.

In this study, a 1D transient model for the frost heave process in a PEFC was formulated to predict the ice lens formation position. The model is a combination and improvement of Harlan's hydraulic model and Miller's rigid ice model, applied to both saturated and unsaturated zones in a PEFC. The GCE, capillary force vs saturation, and the unfrozen water versus temperature characteristic curves are integrated into the model. Additionally, methods to derive these characteristic curves for PEFC diffusion media, catalyst layer, and Nafion membrane, which are critical to the simulation, are given in this paper. Ultimately, this model can be used as a tool to help understand and eventually help mitigate the damage during the freezing process.

Model Formulation

In a PEFC, upon shut down, the diffusion media is typically partially saturated, but with very nonhomogeneous water distribution, and liquid water accumulation favoring locations under the lands.[34] During freezing, it is possible that certain areas become saturated. So the model must incorporate the ice lens initialization and unfrozen water flow in both the fully saturated domain and the unsaturated domain. Thus, a new hybrid model capable of dealing with these physics is needed, and has been formulated.

Model assumptions.— The following assumptions are made for this model.

1. It is a 1D transient model. A BP|BP-CH|DM|CL|Nafion structure is considered here, as shown in Fig. 2. The diffusion media (DM) and catalyst layer (CL) are considered as porous media, and the Nafion (NF) membrane is considered to be a water solvent. The bipolar plate (BP) is considered as a solid. The BP-CH represents the 2D land-channel structure, which is reduced to a 1D heat conductor here. The diffusion media, catalyst layer, and Nafion materials are considered homogeneous and isotropic. Also, there is no freezing induced deformation in the materials, although the model allows for expansion of the ice lenses.

2. Gravity effects can be neglected, compared to the capillary effects in porous media, since through scale analysis, $\rho g(4\pi r^3/3) \ll (2\sigma/r)(\pi r^2)$ for the materials in the PEFC. The multiphase flow in porous media is treated as immiscible, so all continuous phases flow simultaneously through their own tortuous path in the pore space.

3. Around and below freezing temperature, the vapor phase pressure is very small and changes little with temperature, which is much different from the case at 353 K. It is therefore assumed that there is no transport of water vapor. The condensation/vaporization source term and vapor diffusion are neglected. Additionally, without current flow, there is no electro-osmotic transport of water.

4. The porous media can be divided into saturated and unsaturated domains. In the unsaturated domain, air phase pressure is assumed to be constant, since there is no significant flow-induced pressure drop for the air phase. In the saturated domain, it is proposed that the ice lens will appear when the ice phase pressure overcomes the overburden pressure, which will be discussed later. No regelation, or ice flux is considered in our model. Instead, we assume the ice lens growth is caused by the unfrozen water flow into the ice lens. In this way, both the primary frost heave and secondary frost heave can be modeled. Whether the frost front will propagate depends on the balance between the rate of heat loss and unfrozen water flow.

5. The unfrozen water versus temperature curve for the Nafion domain is derived from the best available differential scanning calorimetry (DSC) data for Nafion. For diffusion media and catalyst layer, this curve is calculated using a freezing temperature depression relation and the pore-size distribution. It is assumed that there is always a liquid-like film on the surface of ice, which means the liquid is always the wetting fluid for ice-water flow, even though the backbone material can be mostly hydrophobic. This provides the excepted freezing point depression in the hydrophobic porous media.

6. The Nafion membrane is treated with a pure diffusion model. The diffusion model is chosen based on availability of experimental water diffusivity data. The water content of membrane, λ, is defined as the number of moles of water associated with a mole of sulfonic acid group in the membrane. By using the gradient of λ as the driving force, the diffusion model can be used for the whole range of $0 < \lambda < \lambda_0 = 22$ H_2O/SO_3^-. Actually, if the Nafion can be considered as a porous media with free water at a high water content, (i.e., $22 > \lambda > 14$), through the capillary relation for a two-phase flow in porous media, we can show $\nabla p_w \sim (\partial p_w/\partial s_w)\, \nabla s_w \sim \nabla \lambda$. Thus the hydraulic-type model can be simplified to a diffusion-type model, providing unification of the two approaches. When the Nafion is fully saturated ($\lambda = 22$), the hydraulic-type model is actually the same as a single-phase flow in porous media.

Mass/flow equations.— The mass/flow equation differs between porous media domains and Nafion domain. The porous media domains include diffusion media and catalyst layer. The saturation of air, water, and ice phases, s_a, s_w, and s_i, respectively, have the following relationship

$$s_a + s_w + s_i = 1 \qquad [1]$$

From immiscible flow theories, for water phase, the flow equation can be written as[35]

$$\varepsilon\rho_w\frac{\partial s_w}{\partial t} = \rho_w \nabla \cdot \left(k_{r,w}\frac{k}{\mu_w}\nabla p_w\right) + S_{m,w} \quad [2]$$

where ε is the porosity, k is the intrinsic permeability, $k_{r,w}$ is the relative permeability of the water phase, which changes with the saturation of the water phase, and is defined as $k_{r,w} = k_w/k$,[36] μ_w is the viscosity of water, p_w is the water phase pressure, and $S_{m,w}$ is the mass source term for water phase. For the ice phase, a similar equation can be written. The gas phase equation is neglected, since gas pressure is assumed to be constant, $p_a = p_{ch}$. Also by assumption, there is only water mass transfer between ice and liquid interfaces. So when the flow equations of ice and water phases are added together, the source terms cancel and one can derive

$$\varepsilon\rho_i\frac{\partial s_i}{\partial t} + \varepsilon\rho_w\frac{\partial s_w}{\partial t} = \rho_i\nabla\cdot\left(k_{r,i}\frac{k}{\mu_i}\nabla p_i\right) + \rho_w\nabla\cdot\left(k_{r,w}\frac{k}{\mu_w}\nabla p_w\right) \quad [3]$$

The rigid ice model[20-22] assumed a constant ice flux rate, v_i, which means $(k_{r,i}k/\mu_i)\nabla p_i$ is constant and $\rho_i\nabla\cdot[(k_{r,i}k/\mu_i)\nabla p_i] = 0$. The hydraulic model[14,26,29-32] neglects ice flux therefore $\rho_i\nabla\cdot[(k_{r,i}k/\mu_i)\nabla p_i] = 0$. So both approaches give

$$\varepsilon\rho_i\frac{\partial s_i}{\partial t} + \varepsilon\rho_w\frac{\partial s_w}{\partial t} = \rho_w\nabla\cdot\left(k_{r,w}\frac{k}{\mu_w}\nabla p_w\right) \quad [4]$$

The relative permeability of water phase is usually a function of water saturation, e.g., $k_{r,w} = s_w^3$. In frost heave literature, it's usually a function of saturations of both water and ice phase

$$k_{r,w} = \mathrm{f}(s_w, s_i) \quad [5]$$

In this model, the relative permeability from Jame and Norum[14] or O'Neill and Miller[21] may be most appropriate, considering a lack of experimental data. However, other formulations exist. The proper formulation is not yet known for fuel cell application. Jame and Norum[14] added an impedance term to account for the influence of the ice phase, $k_{r,w} = 10^{-E s_i} s_w^3$. Here, E is the impedance factor and should be around 8–10 for PEFC material, based on the estimation by Gosnik et al.[30] O'Neill and Miller[21] used $k_{r,w} = s_w^9$.

For the boundary conditions, it is assumed that the water migration rate is zero when the diffusion media is next to the bipolar plate, $v_{w,BC} = 0$. When the diffusion media is adjacent to the gas channel, there is a water layer out there with $p_{w,BC} = f(p_{ch}, T)$. For interfaces between different porous media layers and the interface between saturated and unsaturated domains, the phase pressure and flow flux are continuous, which means $p_{w,1} = p_{w,2}$ and $v_{w,1} = v_{w,2}$ for the neighboring grid 1 and 2.

For Nafion domain, water transport has been modeled by many groups. Typically, there are three mechanisms: electro-osmotic drag, diffusion, and capillary flow. During the freezing process, there is no electro-osmotic drag driven by the current flow. For the Nafion model, a pure diffusion model[37-39] is used for the Nafion domain, as introduced in the assumptions

$$\frac{\partial c_w}{\partial t} = \nabla\cdot(D_w\nabla c_w) \quad [6]$$

where, D_w is the diffusivity of water in Nafion and c_w is the water concentration, satisfying $c_w = \lambda c_{acid}$. Here, c_{acid} is the molar concentration of sulfonic acid groups in Nafion.

It has long been established that there are three types of water in Nafion: strongly bound, loosely bound, and free water.[40] The strongly bound water is also the unfreezable water. In the present study, only freezable water is considered. By introducing $\lambda = \lambda_u + \lambda_w + \lambda_i$, water in Nafion can be divided into unfreezable phase, freezable water phase, and ice phase. The unfreezable water content, λ_u, is taken as 2.2 H_2O/SO_3^-.[41] If the Nafion is not freezing, the governing equation is

$$\frac{\partial\lambda_w}{\partial t} = \nabla(D_w\nabla\lambda_w) \quad [7]$$

As water in the Nafion starts to freeze, it becomes

$$\frac{\partial(\lambda_w + \lambda_i)}{\partial t} = \nabla(D_w\nabla\lambda_w) \quad [8]$$

There are two choices on the boundary condition between the porous domain and Nafion domain. It can be set to include the effects of Schroeder's paradox, which is explained by Zawodzinski et al.[42] When the water saturation of the catalyst layer is positive, $s_w > 0$, the membrane is considered to be equilibrated with liquid water with $\lambda_w + \lambda_u = 22$. When $s_w = 0$, the boundary condition is $\lambda_w + \lambda_u = 14$. The second choice is $\lambda_w + \lambda_u = 14 + 8s_w$.

Energy equations.— The energy equations have different forms, depending on position. The 1-D energy equation for the BP and BP-CH domain is

$$\rho C_P\frac{\partial T}{\partial t} = \frac{\partial}{\partial x}\left(\kappa\frac{\partial T}{\partial x}\right) \quad [9]$$

where ρ, C_P, and κ are density, heat capacity, and heat conductivity of the BP or BP-CH domain. The boundary conditions of the fuel cell with the environment can be natural convection or forced convection (e.g., coolant flow) with the heat transfer coefficient $h = h_{NC}$ or h_{FC}.

In porous media domain, the energy equation is written as

$$\frac{D(\overline{\rho C_p}T)}{Dt} = \nabla\cdot(\bar{\kappa}\nabla T) + h_{sf}\frac{D(\varepsilon\rho_i s_i)}{Dt} \quad [10]$$

Thermal properties are calculated as a mixture

$$\overline{\rho C_P} = (\rho_w C_{P,w}s_w + \rho_i C_{P,i}s_i + \rho_a C_{P,a}s_a)\varepsilon + \rho_{pm}C_{P,pm}(1-\varepsilon) \quad [11]$$

$$\bar{\kappa} = (\kappa_w s_w + \kappa_i s_i + \kappa_a s_a)\varepsilon + \kappa_{pm}(1-\varepsilon) \quad [12]$$

where, the subscript *pm* represents both diffusion media and catalyst layer. With the assumptions, there is no ice or gas flux, $v_i = v_a = 0$. In addition, the porous media structure is fixed, $v_s = 0$. The energy equation in the porous media domain simplifies to

$$\frac{\partial(\overline{\rho C_p}T)}{\partial t} + \rho_w C_{p,w}\nabla\cdot(v_w T) = \nabla\cdot(\bar{\kappa}\nabla T) + h_{sf}\varepsilon\rho_i\frac{\partial s_i}{\partial t} \quad [13]$$

The boundary conditions between different domains are continuous, with $q_{dm,BC} = q_{bp-ch,BC}$ and $T_{dm,BC} = T_{bp-ch,BC}$.

In the Nafion domain, similarly, the thermal properties can also be calculated as a mixture. By averaging based on dry Nafion volume, the energy storage coefficient is

$$\overline{\rho C_P} = c_{SO_3^-}M_w[(\lambda_w + \lambda_u)C_{P,w} + \lambda_i C_{P,i}] + \rho_{nf}C_{P,nf} \quad [14]$$

where M_w is the molecular weight of water. The averaged thermal conductivity is

$$\bar{\kappa} = c_{SO_3^-}M_w\left(\frac{\lambda_w + \lambda_u}{\rho_w}\kappa_w + \frac{\lambda_i}{\rho_i}\kappa_i\right) + \kappa_{nf} \quad [15]$$

The conductivity of the mixture, $\bar{\kappa}$, changes more with the ice than water content, since the ice has a much higher conductivity, 1.88 W/m K compared to 0.57 W/m K for water, while the thermal mass parameter, $\overline{\rho C_P}$, depends more on water content, which has a value of 4.22×10^6 J/m^3 K, much higher than the ice phase value of 1.88×10^6 J/m^3 K. This conclusion is also valid for the thermal parameters of porous media domain.

The energy equation with averaged properties in the Nafion domain is

$$\frac{\partial(\overline{\rho C_p}T)}{\partial t} + \rho_w C_{p,w}\nabla\cdot(v_w T) = \nabla\cdot(\bar{\kappa}\nabla T) + h_{sf}c_{SO_3^-}M_w\frac{\partial\lambda_i}{\partial t} \quad [16]$$

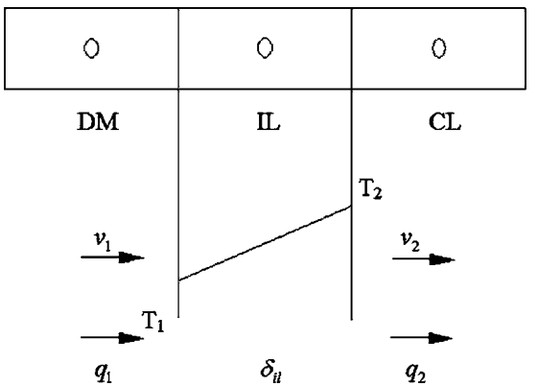

Figure 3. Heat conduction for case with ice lens.

When an ice lens grows in the diffusion media, catalyst layer, or between interfacial layers, it will also influence the local heat transfer. Figure 3 shows the case when ice lens (IL) grows between diffusion media (DM) and catalyst layer (CL). v_1 and v_2 are the water flow rate coming into/out of the ice lens, q_1 and q_2 are heat flux coming into/out of the ice lens, and T_1 and T_2 are temperatures at boundaries of ice lens, and δ_{il} is the thickness of the ice lens. The corrected heat flux is given by

$$q_1 = -\kappa_i \frac{T_2 - T_1}{\delta_{il}} - \rho_w h_{sf} v_1 + \frac{\rho_i C_{P,i} \delta_{il}}{4} \frac{\partial (T_1 + T_2)}{\partial t} \quad [17]$$

$$q_2 = -\kappa_i \frac{T_2 - T_1}{\delta_{il}} - \rho_w h_{sf} v_2 - \frac{\rho_i C_{P,i} \delta_{il}}{4} \frac{\partial (T_1 + T_2)}{\partial t} \quad [18]$$

The ice lens growth rate is determined by

$$\rho_j \frac{d\delta_{il}}{dt} = \rho_w (v_1 - v_2) \quad [19]$$

Characteristic curves.— The rigid ice model[20-22] and the hydraulic model[14,26,29-32] use two of three characteristic curves: (1) the GCE thermodynamic relation; (2) the capillary pressure versus saturation curve; (3) the unfrozen water versus temperature curve. The rigid ice model uses curve 1 and 2, while the hydraulic models uses curve 2 and 3. From soil science studies, calculation results for both models are in reasonable agreement with experimental results, although the thermodynamics of GCE in rigid ice model, and in hydraulic model the permeability impedance factor and similarity on capillary relation have been scrutinized.

In the present model, the following characteristic curves are used for porous media domain: the unfrozen water vs temperature curve for both saturated and unsaturated domain; the GCE relation for both saturated and unsaturated domain; the water/air capillary relation for unsaturated domain. Only the unfrozen water vs temperature curve is needed for the Nafion domain, since it is treated as a water solvent.

The capillary relation between the air phase and water phase is[43]

$$p_{ch} - p_w = \sigma_{aw} \cos \theta_{aw} \sqrt{\varepsilon / k} J(s_e) \quad [20]$$

where σ_{aw} is the surface tension of air-water interface, θ_{aw} is the contact angle, and s_e is the effective saturation, $[s_w/(1 - s_i) - s_{w0}]/(1 - s_{w0})$. The J-Leverett function, $J(s)$, considering a lack of experimental data, is assumed to be[44]

$$J(s) = \begin{cases} 1.417(1-s) - 2.120(1-s)^2 + 1.263(1-s)^3 & \text{wetting fluid} \\ 1.417s - 2.120s^2 + 1.263s^3 & \text{nonwetting fluid} \end{cases} \quad [21]$$

However, no experimental validation of this J-Leverett function for thin-film media of PEFC has been published.

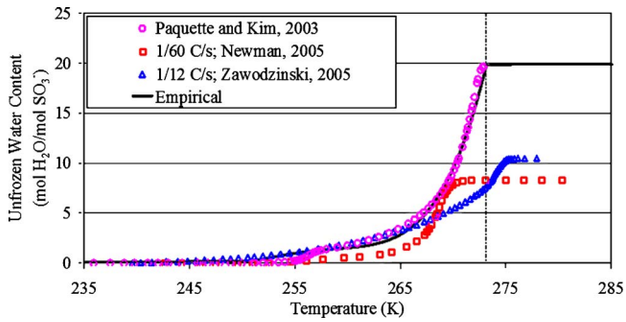

Figure 4. (Color online) Unfrozen water versus temperature curves derived from Nafion DSC data of Ref. 8-11 and 49.

The phase pressure balance between ice and water phases are represented by the GCE, in which h_{sf} is the heat of fusion and T_f is the freezing temperature

$$\frac{p_i}{\rho_i} - \frac{p_w}{\rho_w} = -h_{sf}\left(\frac{T - T_f}{T_f}\right) = -h_{sf}\frac{\Delta T}{T_f} \quad [22]$$

The unfrozen water content in soils decreases continuously with temperature. The finer grained a soil is, the greater the freezing point depression from bulk value. This relation for the Nafion membrane can be extracted from Nafion's differential scanning calorimetry (DSC) data. DSC is one of the methods to measure the unfrozen water versus temperature curve in soil science.[45-48] Also, it has been used to characterize the water composition in Nafion membrane.[9-11,41,49,50] For sake of brevity, detailed discussion on the bonding effects and the methods to derive this curve are not discussed here. Figure 4 shows the unfrozen water versus temperature curves from literature[10,11,49] deemed usable for this purpose.

The empirical equation derived from the data in Fig. 4 is

$$y = \begin{cases} 0 & x < -1 \\ 1 + 5.4x + 11.9x^2 + 11.6x^3 + 4.1x^4 & -1 \leqslant x < 0 \\ 1 & 0 \leqslant x \end{cases} \quad [23]$$

where $x = (T - T_f)/\Delta T = (T - T_f)/24.5$ and $y = \lambda_w/(\lambda_0 - \lambda_u) = \lambda_w/19.8$.

For the diffusion media and catalyst layer, the unfrozen water vs temperature curve can be calculated using their pore size distribution and the freezing temperature depression relation. Through scale analysis, the GCE can be reduced through

$$\frac{\Delta T}{T_f} = -\frac{1}{h_{sf}}\left(\frac{p_i}{\rho_i} - \frac{p_w}{\rho_w}\right) \sim -\frac{1}{h_{sf}}\frac{p_i - p_w}{\rho_i} \sim -\frac{1}{h_{sf}}\frac{p_c}{\rho_i} \sim -\frac{2\sigma_{iw}\cos\theta_{iw}}{h_{sf}\rho_i r^*} \quad [24]$$

This is actually the Gibbs-Thomson equation, which can also be derived from the Gibbs-Duhem equation, but through different approach. This relationship has been used to determine the crystallization temperature of substance in a confined structure.[51] With pore size distribution for Toray carbon paper,[52] one can calculate the volume ΔV of pores with a specific range of Δr^*, in which water has a temperature depression of ΔT, calculated by Eq. 24. After integration, the predicted unfrozen water versus temperature characteristic curve can be obtained, as shown in Fig. 5. Equation 23 can also be used here as an empirical curve with $x = (T - T_f)/\Delta T = (T - T_f)/0.007$, where ΔT is calculated by a pore size of 7 μm, and $y = s_w/s_0 = s_w/1.0$. Similarly, we can use the same equation for catalyst layer with $\Delta T = 0.49$ K, assuming a pore size of 90 nm. The ΔT value we use for Nafion, 24.5 K, is equal to the prediction when the Nafion is treated as a porous media with a pore size of 2 nm.

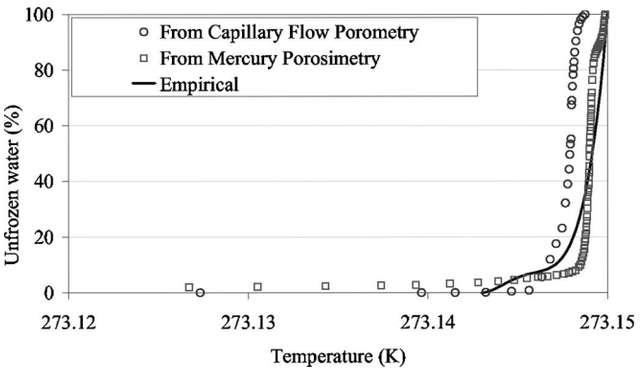

Figure 5. Predicted freezing temperature distribution using pore size distribution data of carbon paper (Toray TGP-H-060) of Ref. 52.

The unknowns of the three characteristic curves are characteristic pressure, p^*, (capillary pressure in capillary relation, $p^* = p_c = p_i - p_w$ for saturated freezing with only water and ice phases, and $p^* = p_{GCE} = p_i/\rho_i - p_w/\rho_w$ in GCE), saturation of wetting fluid s_w, and temperature T. p_c is usually a function of both s_w and T.[53,54] By constructing the unfrozen water relation (Eq. 23), and capillary pressure relation $p_c = p_i - p_w = \sigma_{iw}\cos\theta_{iw}\sqrt{\varepsilon/kJ(s_w)}$ with Leverett function (Eq. 21), in a (p_c,s_w,T) space, one can derive the curve $p_c(s_w,T)$, shown in Fig. 6. This type of curve has been derived by Haeupl and Xu.[54] They used the curve to calculate the maximum unfrozen water as a function of temperature and water saturation in concrete block. During freezing, the capillary pressure follows both the capillary force versus saturation curve ($p_c \sim s_w$) and the unfrozen water versus temperature curve ($s_w \sim T$). The importance of the curve is that it will be following a $p_c \sim T$ relation, which was not discussed by Haeupl and Xu. It actually represents a thermodynamic relation similar to GCE. However it is not exactly the GCE. If we used the GCE $p_{GCE} = (p_i/\rho_i - p_w/\rho_w) \sim T$ and $s_w \sim T$ curve, a similar $p_{GCE}(s_w,T)$ can be drawn. $p_c(s_w,T)$ and $p_{GCE}(s_w,T)$ differ because $p_c \sim s_w$ and $s_w \sim T$ are all empirical curves, and data points were fit using $p_c = p_i - p_w$, instead of $p_{GCE} = p_i/\rho_i - p_w/\rho_w$. By further studying the situation for hydrophilic and hydrophobic porous media, they will have similar curves, which means the liquid phase is always the wetting fluid even for hydrophobic porous media. This result is very compatible with the modern premelting theory[55,56] that there is always a liquid-like film on top of ice with thickness depending on temperature, and thus water trapped in porous media always has a freezing temperature depression. This was also observed through experiments by Sage and Porebska,[57] in which hydrophobic and hydrophilic soil samples with same grain size distribution have similar freezing temperature depression.

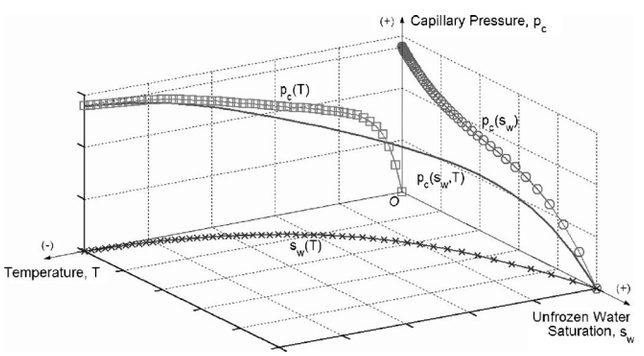

Figure 6. Dependence of capillary pressure on water content and temperature, in which -×- represents the unfrozen water versus temperature curve, -o- represents the capillary pressure versus saturation curve, -□ represents the thermodynamic relation, the unmarked one is the $p_c(s_w,T)$ curve.

Table I. Local overburden pressure.

Position	Under BP	Under CH
Within diffusion media (DM), catalyst layer (CL), or Nafion	$P_{ovbd} = P_{assm} + \sigma_{ts} + p_{ch}$	$P_{ovbd} = p_{ch} + \sigma_{ts} + \tau_{sh}$
At interface between bipolar plate (BP)|DM, DM|CL, or CL|Nafion	$P_{ovbd} = P_{assm} + p_{ch}$	$P_{ovbd} = p_{ch} + \tau_{sh}$

Thus, for saturated freezing, the three types of characteristic curves actually represent a single relation, $p^*(s_w,T)$. So it is not unexpected that the rigid ice model and the hydraulic model can both give accurate simulation results, since they interpret the same physics differently by using two of the three characteristic curves. Together with the saturation relation (Eq. 1), flow equation (Eq. 4), and energy equation, (Eq. 10), a closed system for five unknowns can be formed for a saturated system. For the rigid ice model, the unknowns are p_w, p_i, s_w, s_i, and T. The frost heave rate, v_{fh}, is calculated by assuming an additional boundary condition, constant ice flux. For the hydraulic model, the unknowns are then p_c, s_w, s_i, T, and v_{fh}. By modifying the flow equation (Eq. 4), the frost heave rate can also be solved, though this approach has not been published to our knowledge. Harlan[24] only used one characteristic curve for his saturated model, so his model is not able to solve the frost heave rate.

For an unsaturated system, there is an additional unknown, s_a. The hydraulic model is able to deal with the problem by solving a system of p_c, s_w, s_i, s_a, and T, as an ice lens is not supposed to appear in unsaturated zone and v_{fh} can be neglected. The rigid ice model has not been applied in unsaturated zone. In this study, we use their concept of phase pressure and similar frost heave initialization criteria, which will be discussed next. The PEFC system modeled then has seven unknowns: p_w, p_i, p_a, s_w, s_i, s_a, and T. By assuming constant gas phase pressure and using the capillary relation between air and water phase (Eq. 20), we can extend the rigid ice model for the unsaturated case of the PEFC diffusion media and catalyst layer with seven equations total.

Ice lens initialization.— The initialization of ice lens occurs when the ice pressure reaches the local overburden pressure, P_{ovbd}. The concept of overburden pressure here is actually a critical ice lens formation pressure. Only when the ice phase pressure is greater than the critical ice lens formation pressure, the ice lens can initialize

$$P_{ovbd} = p_i \qquad [25]$$

This also serves as the boundary condition for the capillary flow at ice lens surface. The local overburden pressure will depend on the location. All the possible cases for overburden are listed in Table I, where P_{assm} is the assembling pressure for PEFC, σ_{ts} is the material tensile strength, and τ_{sh} is shear stress, generated by the diffusion media deformation in the through-plane direction, which also depends on the ice lens thickness.

Discussion

The freezing process may cause several problems to a PEFC. Possible ice lens positions are shown in Fig. 7. Ice could block the flow channels and prevent reactants reaching catalyst layer; increase the thermal mass of the total system and slow down the heat-up process; increase the electrical/thermal contact resistance by delaminating the interfaces of PEFC components; reduce the active elec-

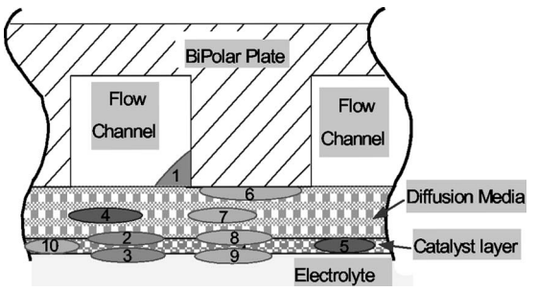

Figure 7. Schematic showing the potential locations of freeze/thaw damage. Ice lenses grow most likely in locations 1-3 and possibly 9, less likely in locations 4–5, and not likely in locations 6–8 and 10.

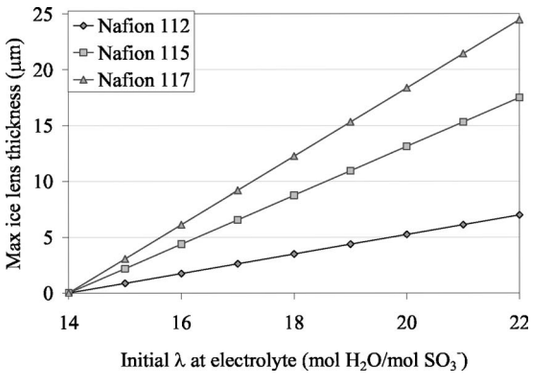

Figure 8. Maximum thickness of ice lens that could be formed by water expelled from Nafion during freezing, as a function of the initial water content and membrane type, if the boundary condition is saturated with water vapor and $\lambda = 14$ H_2O/SO_3^-.

trochemical surface area by damaging the catalyst layer; or increase the crossover rate of reactants by damaging the membrane structure.

Predictions on ice lens location (why diffusion media can suffer breakthrough damage).— By Eq. 20 and 21, $|p_0 - p_w| = \sigma_{aw}|\cos\theta_{aw}|\sqrt{\varepsilon/kJ(S_e)} < 0.6\sigma_{aw}\sqrt{\varepsilon/k}$. For typical diffusion media $k = 5.5 \times 10^{-11}$ m^2 and $\varepsilon = 0.7$,[52] together with $\sigma_{aw} = 0.07$ Pa·m,[16] $|p_0 - p_w| < 5$ kPa. For catalyst layer, there is no published data for permeability. By using Carman-Kozeny equation, $k = (r^*)^2\varepsilon^3/18\tau(1-\varepsilon)^2$, with $\varepsilon = 0.7$, $r^* = 270$ nm, and $\tau = 1.52$,[58] it is estimated $k = 1.0 \times 10^{-14}$ m^2 and $|p_0 - p_w| < 0.35$ MPa. Therefore, the water phase pressure should be less then 0.11 MPa for diffusion media and 0.45 MPa for catalyst layer. By Eq. 22, ice phase pressure can be estimated by $p_i = \rho_i(p_w/\rho_w - h_{sf}\Delta T/T_f)$. The freezing temperature depression is 0.007 K for diffusion media and 0.545 K for catalyst layer, so p_i is less then 0.11 MPa for diffusion media and 1.1 MPa for catalyst layer. The assembling pressure of a typical fuel cell, P_{assm}, is usually >1 MPa of lands onto diffusion media,[59] so the ice lens is not likely to grow under the lands, to locations 6–8 and 10 in Fig. 7. Location 9 is an exception, since the ice phase pressure inside Nafion or at CL/Nafion could be very large, $\gg 1$ MPa, due to the large freezing temperature depression of 24.5 K in Nafion. The tensile strength of diffusion media is 0.01–0.1 MPa,[60] and data for catalyst layer is expected to be less or similar, so the ice lens is less likely to grow within the diffusion media (DM) and catalyst layer (CL) under the channels, locations 4–5 in Fig. 7. For interface of CL|Nafion and DM|CL under channel, or DM|channel, location 1-3 in Fig. 7, the ice lens is most likely to occur, because the overburden pressure is relatively small.

Thus, the ice lens formed around the catalyst layer under the channel can grow and break through the diffusion media into the channel by shear forces. A thick ice lens means large deformation and large stress force on the diffusion media. Additionally, the carbon paper is more easy to damage via this mode as it is more brittle in shear than carbon cloth.

Water expelled from Nafion (possible explanation for delamination between Nafion and catalyst layer).— From the unfrozen water relation, the Nafion has a relatively large freezing temperature depression (~24.5 K), so the unfrozen water can flow out of the Nafion, well below the freezing point of the catalyst layer. Liquid water coming out would freeze instantly in the catalyst layer, and an ice lens can grow when pores are saturated with ice and ice phase pressure overcomes the overburden pressure. An estimation was made for the maximum thickness of ice lens formed from only water ejected from Nafion on freezing. The maximum thickness produced by this effect is a function of initial water content and membrane type, as shown in Fig. 8. The boundary of Nafion is assumed to be saturated with water vapor with $\lambda = 14$. Since the catalyst layer is ~15 μm, and lens thickness can reach the same magnitude from Fig. 8, the ice lens formed by this mode could be a significant source for damage. Additionally, the Nafion thickness has direct effects on the potential damage in this mode.

Factors affecting ice lens growth.— During the frost heave process, there usually exists a frozen fringe, with ice content from 0% to 100%. The unfrozen water flow takes place mostly in the frozen fringe. The wider the frozen fringe, the thicker an ice lens can grow. The thickness of the frozen fringe increases with lower overburden pressures and low temperature gradients. Also, residual water saturation and distribution play key roles in the frost heave process. With greater initial water saturation, the frost heave will occur more readily, thus, proper purging of the fuel cell on shut down is critical. Finally, higher water permeability of the porous media can permit greater water flux to the ice lens location, increasing the frost heave rate. Thus, steady state residual water content is a critical issue for mitigation of freeze-thaw damage.

There are several methodologies to influence the ice lens formation in a PEFC, which include: *(i)* control the temperature gradient after shutdown, *(ii)* control the overburden pressure to influence the freezing fringe range and ice lens growth rate, *(iii)* modify purging protocols to reduce residual water to acceptable levels, and *(iv)* engineer the flow fields or modify material properties for bipolar plates, diffusion media, and catalyst layer, to reduce the residual water at shutdown. Work is ongoing at the FCDDL to code the formulated model and perform a parametric study of frost heave in PEFC, as well as experimentally validate results using a variety of techniques.

Conclusions

In this work, a 1D transient freezing model to describe the water migration and ice lens formation process has been formulated, based on theories of porous media flow and soil frost heave mechanisms. The freezing process in a PEFC is mostly an unsaturated freezing process, although it is also possible that certain areas become saturated. Then ice lenses grow. The present model is a hybrid and extension of Harlan's hydraulic model and Miller's rigid ice model for frost heave in soils, which can be applied to both saturated and unsaturated domains in PEFCs. The model also relies on several characteristic curves derived, or used from literature to describe the p_c, s_w, and T relationships. It is found that the three types of characteristic curves for unfrozen water flow and frost heave modeling can be well unified. For Nafion, the unfrozen water versus temperature curve can be derived from available DSC data. For the diffusion media and the catalyst layer, this curve can be predicted through freezing temperature depression and pore size distribution data. Through the characteristic curves and formulated model, it is predicted that ice lens formation is most likely around the catalyst layer,

either between catalyst and diffusion media, or between catalyst layer and Nafion membrane, under the channel but not the lands. An exception is that ice lenses could appear at CL/Nafion under lands as a result of the large freezing temperature depression of Nafion. This mode can explain breakthrough damage observed in carbon paper after freeze-thaw tests. Additionally, the unfrozen water can continuously flow out of the Nafion, though at a relatively small rate. The ice lens formed from this water source could be a significant source for delamination damage between Nafion and catalyst layer. The Nafion thickness and initial water content have a direct effect on the potential damage by this mode.

Acknowledgments

This research was supported by the Advanced Technology Center, R&D Division for Hyundai Motor Company and Kia Motors Corporation (HMC&KMC).

Pennsylvania State University assisted in meeting the publication costs of this article.

List of Symbols

c	molar concentration, mol/L
C_P	specific heat capacity, J/kg K
D	diffusivity, m/s^2
E	impedance factor of permeability
g	acceleration of gravity, 9.8 m/s^2
h	heat transfer coefficient,W/m^2 K
h_{sf}	water's heat of fusion, J/kg
J	J-Leverett function
k	permeability, m^2
k_r	relative permeability
M	molar weight, g/mol
p	phase pressure, Pa
p^*	characteristic pressure
P	pressure, Pa
q	1-D heat flux, W/m^2
r	mean radius, m
r^*	capillary tube radius, m
s	saturation
s_u	maximum unfrozen water saturation
S_m	mass source, kg/m^3 s
t	time, s
T	temperature, K
T_f	freezing temperature, K
v	velocity, m/s
V	volume, m^3 or Voltage, V

Greek

δ	thickness, m
ε	porosity
κ	thermal conductivity, W/m K
$\bar{\kappa}$	averaged thermal conductivity, W/m K
λ	water content in Nafion, mol H_2O/mol SO_3^-
μ	viscosity, Pa s
θ	contact angle, degree
ρ	density, kg/m^3
ρC_P	averaged storage term parameter for energy equation, J/m^3 K
σ	surface tension, Pa m
σ_{ts}	tensile strength, Pa
τ	tortuosity
τ_{sh}	shear stress, Pa

Subscripts

0	reference point
a	air phase
acid	sulfonic acid group
assm	assembling
BC	boundary condition
bp	bipolar plate
c	capillary
ch	channel
cl	catalyst layer
dm	diffusion media
fh	frost heave
FC	forced convection
GCE	GCE relation
i	ice phase
il	ice lens
NC	natural convection
nf	Nafion membrane
ovbd	overburden
pm	porous media
s	solid phase
u	unfreezable water
w	freezable water in Nafion; water phase in other case

References

1. M. S. Wilson, J. A. Valerio, and S. Gottesfeld, *Electrochim. Acta*, **40**, 355 (1995).
2. R. C. McDonald, C. K. Mittelsteadt, and E. L. Thompson, *Fuel Cells*, **4**, 208 (2004).
3. L. Blair, in http://www.eere.energy.gov/hydrogenandfuelcells/fc_freeze_workshop.html
4. B. Pivovar, in http://www.eere.energy.gov/hydrogenandfuelcells/fc_freeze_workshop.html
5. E. Cho, J.-J. Ko, H. Y. Ha, S.-A. Hong, K.-Y. Lee, T.-W. Lim, and I.-H. Oh, *J. Electrochem. Soc.*, **150**, A1667 (2003).
6. E. Cho, J.-J. Ko, H. Y. Ha, S.-A. Hong, K.-Y. Lee, T.-W. Lim, and I.-H. Oh, *J. Electrochem. Soc.*, **151**, A661 (2004).
7. Y. S. Kim, in http://www.hydrogen.energy.gov/annual_review05_fuelcells.html
8. J. Newman, in http://www.hydrogen.energy.gov/annual_review05_fuelcells.html
9. T. A. Zawodzinski, in http://www.eere.energy.gov/hydrogenandfuelcells/fc_freeze_workshop.html
10. R. Gaylord, in http://www.eere.energy.gov/hydrogenandfuelcells/fc_freeze_workshop.html
11. J. P. Meyers, in http://www.eere.energy.gov/hydrogenandfuelcells/fc_freeze_workshop.html
12. A. A. Pesaran, G.-H. Kim, J. D. Gonder, in http://www.nrel.gov/hydrogen/proj_fuelcells.html
13. C. Dirksen and R. D. Miller, *Soil Sci. Soc. Am. Proc.*, **30**, 168 (1966).
14. Y. W. Jame and D. I. Norum, *Water Resour. Res.*, **16**, 811 (1980).
15. T. Mizusaki and M. Hiroi, *Physica B*, **210**, 403 (1995).
16. R. D. Miller, in *Applications of Soil Physics*, D. Hillel, Editor, p. 254, Academic Press, New York (1980).
17. K. O'Neill, *Cold Regions Sci. Technol.*, **6**, 275 (1983).
18. P. B. Black and M. J. Haradenberg, CRREL Report 91-23, p. 1, U.S. Army Cold Region Research and Engineering Laboratory, Hanover, NH (1991).
19. Y. Nakano, *Cold Regions Sci. Technol.*, **29**, 9 (1999).
20. R. D. Miller, in *Proceedings of the 3rd International Conference on Permafrost*, National Research Council of Canada, p. 708 (1978).
21. K. O'Neill and R. D. Miller, *Water Resour. Res.*, **21**, 281 (1985).
22. P. B. Black, CRREL Report 95-12, p. 1, U.S. Army Cold Region Research and Engineering Laboratory, Hanover, NH (1995).
23. J. P. G. Loch, *Soil Sci.*, **126**, 77 (1978).
24. K. S. Henry, CRREL Report TR-00-16, p. 1, U.S. Army Cold Region Research and Engineering Laboratory, Hanover, NH (2000).
25. K. S. Førland, T. Førland, and S. Ratkje, *Irreversible Thermodynamics Theory and Applications*, p. 235, John Wiley and Sons, New York (1988).
26. G. P. Newman and G. W. Wilson, *Can. Geotech. J.*, **34**, 63 (1997).
27. A. P. S. Selvadurai, J. Hu, and I. Konuk, *Cold Regions Sci. Technol.*, **29**, 215 (1999).
28. A. W. Rempel, J. S. Wettlaufer, and M. G. Worster, *J. Fluid Mech.*, **498**, 227 (2004).
29. R. L. Harlan, *Water Resour. Res.*, **9**, 1314 (1973).
30. J. P. Gosnik, K. Kawasaki, T. E. Osterkamp, and J. Holty, in *Proceedings of the 5th International Conference on Permafrost*, Tapir Publishers, p. 355 (1988).
31. L. Zhao and D. M. Gray, *ASME, Heat Trans. Div.*, **331**, 53 (1996).
32. S. A. Shoop and S. R. Bigl, *Cold Regions Sci. Technol.*, **25**, 33 (1997).
33. D. G. Fredlund, A. Xing, and S. Huang, *Can. Geotech. J.*, **31**, 533 (1994).
34. P. A. Chuang, A. Turhan, A. K. Heller, J. S. Brenizer, T. A. Trabold, and M. M. Mench, in *Proceedings of the 3rd International Conference on Fuel Cell Science, Engineering and Technology* (2005).
35. T. Dracos, in *Modelling and Applications of Transport Phenomena in Porous Media*, J. Bear and J.-M. Buchlin, Editors, p. 195, Kluwer Academic Publishers, Boston (1991).
36. A. H. Demond and P. V. Roberts, *Water Resour. Bull.*, **23**, 617 (1987).
37. T. E. Springer, T. A. Zawodzinski, and S. Gottesfeld, *J. Electrochem. Soc.*, **138**, 2334 (1991).
38. S. Motupally, A. J. Becker, and J. W. Weidner, *J. Electrochem. Soc.*, **147**, 3171 (2000).
39. G. J. M. Janssen, *J. Electrochem. Soc.*, **148**, A1313 (2001).
40. K. A. Mauritz and R. B. Moore, *Chem. Rev. (Washington, D.C.)*, **104**, 4535 (2004).
41. Y. S. Kim, L. Dong, M. A. Hickner, T. E. Glass, V. Webb, and J. E. McGrath, *Macromolecules*, **36**, 6281 (2003).
42. T. A. Zawodzinski, C. Derouin, S. Radzinski, R. J. Sherman, V. T. Smith, T. E. Springer, and S. Gottesfeld, *J. Electrochem. Soc.*, **140**, 1041 (1993).
43. J. Bear, *Dynamics of Fluids in Porous Media*, p. 439, American Elsevier, New York (1972).
44. K. S. Udell, *Int. J. Heat Mass Transfer*, **28**, 485 (1985).
45. L. Bronfenbrener and E. Korin, *Chem. Eng. Process.*, **41**, 357 (2002).
46. D. M. Anderson and A. R. Morgenstern, in *Proceedings of 2nd International Conference on Permafrost, North American Contribution*, National Academy of Sciences, p. 257 (1973).

47. F. Civan, *J. Cold Regions Eng., Cold Regions Sci. Technol.*, **14**, 146 (2000).
48. T. Kozlowski, *J. Cold Regions Eng., Cold Regions Sci. Technol.*, **36**, 71 (2003).
49. J. W. Paquette and K. J. Kim, in *Proceedings of 2003 ASME International Mechanical Engineering Congress and Exposition*, ASME, p. 205 (2003).
50. M. Saito, K. Hayamizu, and T. Okada, *J. Phys. Chem. B*, **109**, 3112 (2005).
51. C. Faivre, D. Bellet, and G. Dolino, *Eur. Phys. J. B*, **7**, 19 (1999).
52. M. F. Mathias, J. Roth, J. Fleming, and W. Lehnert, in *Handbook of Fuel Cells—Fundamentals, Technology and Applications*, W. Vielstich, A. Lamm, and H. A. Gasteiger, Editors, p. 517, John Wiley & Sons, New York (2003).
53. J. Bachmann, R. Horton, S. A. Grant, and R. R. Van der Ploeg, *Soil Sci. Soc. Am. J.*, **66**, 44 (2002).
54. P. Haeupl and Y. Xu, *J. Thermal Envelope Bldg. Sci.*1097-1963, **25**, 4 (2001).
55. J. D. Dash, in *Ice Physics and the Natural Environment*, J. S. Wettlaufer, J. G. Dash, and N. Untersteiner, Editors, p. 11, Springer, New York (1999).
56. L. A. Wilen and J. G. Dash, *Phys. Rev. Lett.*, **74**, 5076 (1995).
57. J. D. Sage and M. Porebska, *J. Cold Reg. Eng.*, **7**, 99 (1993).
58. H. S. Salem and G. V. Chilingarian, *Energy Sources*, **22**, 207 (2000).
59. W.-K. Lee, C.-H. Ho, J. W. Van Zee, and M. Murthy, *J. Power Sources*, **84**, 45 (1999).
60. http://www.etek-inc.com